International Journal of Modern Physics D
Vol. 13, No. 9 (2004) 1955–1972

World Scientific
www.worldscientific.com

PROPERTIES OF ACCRETION SHOCKS IN VISCOUS FLOWS WITH COOLING EFFECTS

SANTABRATA DAS* and SANDIP K. CHAKRABARTI†
S.N. Bose National Centre for Basic Sciences,
JD-Block, Sector III, Salt Lake, Kolkata 700098, India
**sbdas@bose.res.in*
†*chakraba@bose.res.in*

Received 9 April 2004
Communicated by B. S. Sathyaprakash

Low angular momentum accretion flows can have standing and oscillating shock waves. We study the region of the parameter space in which multiple sonic points occur in viscous flows in presence of various cooling effects such as bremsstrahlung and Comptonization. We also quantify the parameter space in which shocks are steady or oscillating. We find that cooling induces effects opposite to heating by viscosity even in modifying the topology of the solutions, though one can never be exactly balanced by the other due to their dissimilar dependence on dynamic and thermodynamic parameters. We show that beyond a critical value of cooling, the flow ceases to contain a shock wave.

Keywords: Black hole physics; accretion; jets and outflows.

1. Introduction

Cooling and heating processes play an important role in studying the accretion disks around compact objects. In this paper, we consider both viscous heating and bremsstrahlung cooling as energy dissipative processes. In Chakrabarti and Das,[1] the problem of accretion and winds with small angular momentum was solved in a very comprehensive way when viscous heating was included. The entire parameter space was scanned and separated in terms of flows with and without shocks. A major scope for further work is to find and separate the parameter space which allows shock formations when cooling effects are also included. This will allow us to study flows with high accretion rate as well. The question arises because viscosity transports angular momentum and increases the possibility of shock formation at a larger distance from the black hole. However, cooling reduces the post-shock pressure and therefore the possibility of shock formation. Various cooling processes will and should change the parameter space in which shocks form.

†Also at Centre for Space Physics, Chalantika 43, Garia Station Rd., Kolkata 700084.

In Chakrabarti,[2] some of the effects of cooling was included. Assuming that cooling at a given radius of an accretion disk is proportional to the heating, all possible topologies were presented. While cooling will and should depend on heating, there is no reason to believe that this proportionality is independent of radial distance. It is therefore necessary to re-visit the problem with explicit form of heating and cooling included.

In the present paper, we make these important extensions of the previous work and show that shocks are still possible in a very large part of the parameter space. We find topologies of solutions which are similar to what was found for spiral shock study,[3] but otherwise new for axisymmetric situation. We also find new topologies which were not anticipated before. In more recent years, it has become evident that the standing shocks may be very important in explaining the spectral properties of black hole candidates[4] as the post-shock region behaves as the boundary layer where accreting matter dissipates its thermal energy and generates hard X-ray by inverse Comptonization. This region is also found to be responsible to produce relativistic outflows. Furthermore, numerical simulations indicated that the shocks may be oscillating at nearby regions of the parameter space in presence of cooling effects[5] and the shock oscillations can also explain intricate properties of quasi-periodic oscillations.[6] Recent observations do support the presence of sub-Keplerian flows in accretion disks.[7,8]

The present work is done around a Schwarzschild black hole by using pseudo-Newtonian potential.[9] We use a similar viscosity prescription as in Chakrabarti.[2] In Section 2, we present model equations which included both heating and cooling effects. In Section 3, we perform the sonic point analysis. In Section 5, we study the nature of the sonic points and how they vary with flow parameters. In Section 6, we study the global solution topologies with heating and cooling effects. In Section 7, we classify the parameter space in terms of whether shocks will form or not and how it depends on flow parameters. In Section 8, we briefly report how even the super-Keplerian flows may also be transonic. Finally, in Section 9, we discuss the importance of these solutions and make concluding remarks.

2. Model Equations When Cooling Effects are Included

As far as the cooling processes are concerned, they could be due to various physical reasons, such as the thermal and the non-thermal bremsstrahlung, synchrotron, Comptonization, etc. For simplicity, we assume that the Comptonization enhances the injected photon intensity due to bremsstrahlung by a factor of ζ which can take any value from 1 to $\sim$ few $\times$ 100 depending on the availability of soft photons.[4] In other words, we use ζ as a parameter to represent the net cooling.

We start with a thin, axisymmetric, rotating viscous accretion flow around a Schwarzschild black hole. The space–time geometry around a non-rotating black hole can be satisfactorily described by the pseudo-Newtonian potential[9] and is given by $g(x) = -\frac{1}{2(x-1)}$, where, x is the radial distance in dimensionless unit.

In the steady state, the dimensionless hydrodynamic equations that govern the infalling matter are the followings:[2]

(a) Radial momentum equation:

$$\vartheta\frac{d\vartheta}{dx}+\frac{1}{\rho}\frac{dP}{dx}-\frac{\lambda(x)^2}{x^3}+\frac{1}{2(x-1)^2}=0\,. \tag{1a}$$

(b) Baryon number conservation equation:

$$\dot{M}=\Sigma\vartheta x\,, \tag{1b}$$

apart from the geometric constant.

(c) Angular momentum conservation equation:

$$\vartheta\frac{d\lambda(x)}{dx}+\frac{1}{\Sigma x}\frac{d}{dx}(x^2W_{x\phi})=0\,. \tag{1c}$$

(d) The entropy generation equation:

$$\Sigma\vartheta T\frac{ds}{dx}=Q^+-Q^-\,. \tag{1d}$$

Here, ϑ is the radial velocity and $\lambda(x)$ is the specific angular momentum of the flow. The distances, velocities and masses are made dimensionless by using $r_g = 2GM_{\rm BH}/c^2$, the Schwarzschild radius, c, the velocity of light and $M_{\rm BH}$, the mass of the black hole, respectively. Here Σ and $W_{x\phi}$ are the vertically integrated density and viscous stress, s is the entropy density of the flow, T is the local temperature, Q^+ and Q^- are the heat gained and lost by the flow, and $\dot{M}$ is the mass accretion rate. We assume that the accretion flow is in hydrostatic equilibrium in the vertical direction and the vertical velocity component is much smaller compared to the radial component. With this assumption, the local disk height is obtained by equating the pressure gradient force in the vertical direction with the gravitational force. The half thickness of the disk is then given by

$$h(x)=ax^{1/2}(x-1)\,, \tag{2}$$

where the sound speed is defined as $a=\sqrt{\gamma P/\rho}$, where γ, P and ρ being the adiabatic index, pressure and density respectively.

In the present paper, we follow a similar viscosity prescription as given in Chakrabarti[2] where $W_{x\phi}=-\alpha_\Pi\Pi$ is used. This prescription ensures that viscous stress remain continuous at the flow discontinuity (shock) in presence of significant radial motion of the accretion flow.

3. Sonic Point Analysis

A black hole accretes matter either from its binary companion or from the surrounding ambient medium. This matter starts with a negligible radial velocity at the outer edge of the disk. But it enters into the black hole with the velocity of light.[10] This ensures that inside the accretion disk there must be at least one point

where the radial velocity exactly matches with the sound speed. This point is known as the sonic point. Accretion flow which passes through a shock wave must cross sonic points at least twice. In other words, the flow may be called multi-transonic.

For the accretion flow, entropy equation (1d) can be simplified as

$$\frac{\vartheta}{\gamma-1}\left[\frac{1}{\rho}\frac{dP}{dx}-\frac{\gamma P}{\rho^2}\frac{d\rho}{dx}\right]=\frac{Q^- - Q^+}{\rho h}=C-H\,. \tag{3}$$

and then $H(=Q^+/\rho h)$ takes the form,

$$H=Ax(ga^2+\gamma\vartheta^2)\frac{d\Omega}{dx}\,, \tag{4}$$

where, $A=-\alpha_\Pi\frac{I_n}{\gamma}$ and $g=\frac{I_{n+1}}{I_n}$. Here, $\Omega(x)$ is the angular velocity of the accreting matter at the radial distance x, n is the polytropic index $\left(n=\frac{1}{(\gamma-1)}\right)$. The general expression of I_n is given by[11]

$$I_n=\frac{(2^n n!)^2}{(2n+1)!}\,. \tag{5}$$

Simultaneously with viscous heating, we use Comptonization of the bremsstrahlung radiation as the physical cooling process. The following analysis is carried out with non-dimensional cooling term $C(=Q^-/\rho h)$ as

$$C=\frac{\zeta B}{\vartheta x^{3/2}(x-1)}\,, \tag{6a}$$

with

$$B=1.4\times10^{-27}\left(\frac{\mu m_p}{2k}\right)^{1/2}\frac{\dot{M}}{2\pi m_p^2}\frac{1}{2GcM_{\rm BH}}\,, \tag{6b}$$

where μ is the mean molecular weight, m_p is the mass of the proton and k is the Boltzmann constant respectively.

3.1. *Sonic point condition*

From Eqs. (1a)–(1d), the sonic point conditions are derived following the general procedure[12] and are given by

$$\frac{d\vartheta}{dx}=\frac{N}{D}\,, \tag{7}$$

where the numerator N is

$$N=-\frac{\alpha_\Pi A(a^2g+\gamma\vartheta^2)^2}{\gamma x}-\left[\frac{\lambda^2}{x^3}-\frac{1}{2(x-1)^2}\right]$$
$$\times\left[2\alpha_\Pi gA(a^2g+\gamma\vartheta^2)+\frac{(\gamma+1)\vartheta^2}{(\gamma-1)}\right]$$

$$- \frac{\vartheta^2 a^2(5x-3)}{x(\gamma-1)(x-1)} - \frac{\alpha_\Pi g A a^2(5x-3)(a^2 g+\gamma\vartheta^2)}{\gamma x(x-1)} + \frac{2\lambda A\vartheta(a^2 g+\gamma\vartheta^2)}{x^2} + \frac{B}{x^{3/2}(x-1)}\,, \tag{8a}$$

and the denominator D is

$$D = \frac{2a^2\vartheta}{(\gamma-1)} - \frac{(\gamma+1)\vartheta^3}{(\gamma-1)} - A\alpha_\pi\vartheta(a^2 g+\gamma\vartheta^2)\left[(2g-1) - \frac{a^2 g}{\gamma\vartheta^2}\right]. \tag{8b}$$

At the sonic point, both the numerator and denominator vanish. For $D = 0$, one can get the expression for the Mach Number $M(x_c)$ at the sonic point which is given by,

$$M(x_c) = \sqrt{\frac{-m_b - \sqrt{m_b^2 - 4m_a m_c}}{2m_a}} \approx \sqrt{\frac{2}{\gamma+1}} \quad \text{for} \quad \alpha_\Pi \to 0\,, \tag{9}$$

where,

$$m_a = -A\alpha_\Pi\gamma^2(\gamma-1)(2g-1) - \gamma(\gamma+1)\,, \tag{10a}$$

$$m_b = 2\gamma - 2A\alpha_\pi g\gamma(\gamma-1)(g-1)\,, \tag{10b}$$

$$m_c = A\alpha_\pi g^2(\gamma-1)\,. \tag{10c}$$

In order for the Mach number to be physically acceptable, we do not use the negative sign within the square root. In the weak viscosity limit, Mach number at the sonic point reduces to the result as obtained in Chakrabarti.[12]

Setting $N = 0$, we get an algebraic equation for sound speed at the sonic point which is given by

$$F(\mathcal{E}_c, \lambda_c, x_c) = \mathcal{A}a^4(x) + \mathcal{B}a^3(x) + \mathcal{C}a^2(x) + \mathcal{D} = 0\,, \tag{11}$$

where,

$$\mathcal{A} = -\left[\frac{\alpha_\Pi A\{g+\gamma M^2\}^2}{\gamma x} + \frac{\alpha_\Pi A(5x-3)\{g+\gamma M^2\}}{\gamma x(x-1)} + \frac{M^2(5x-3)}{x(\gamma-1)(x-1)}\right], \tag{12a}$$

$$\mathcal{B} = \frac{2\lambda A M(g+\gamma M^2)}{x^2}\,, \tag{12b}$$

$$\mathcal{C} = -\left[\frac{\lambda^2}{x^3} - \frac{1}{2(x-1)^2}\right]\left[2\alpha_\Pi g A(g+\gamma M^2) + \frac{(\gamma+1)M^2}{(\gamma-1)}\right], \tag{12c}$$

$$\mathcal{D} = \frac{B}{x^{3/2}(x-1)}\,. \tag{12d}$$

We solve the above quadratic equation to obtain the sound speed at the sonic point. Das, Chattopadhyay and Chakrabarti[13] found that depending on a given set of initial parameters, accretion flow may have a maximum of four sonic points where one of the sonic points always lies inside the black hole horizon for non-dissipative accretion flow.[10,13] In our present study, we also expect a similar result if we are

interested in the weak viscosity and weak cooling limit. Below, we study the nature of the sonic points.

4. Nature of the Sonic Points

Accreting matter begins subsonically from the outer edge of the disk and becomes supersonic after passing through the sonic point before entering into black hole. A flow may contain multiple sonic points depending on the initial set of input parameters. Nature of sonic points depends on the value of the velocity gradients $(d\vartheta/dx)$ at the sonic points. At each sonic point, $(d\vartheta/dx)$ has distinctly two different values. If both the velocity gradients are real and of opposite signs, the sonic points is saddle type and one is used for accretion and the other used for winds. Nodal type sonic point belongs to the class when the derivatives are real and of the same sign. When the derivatives are complex, the sonic point is of spiral type. For a standing shock to form, an accretion flow must have more than one saddle type sonic point.

In Fig. 1(a), we plot the variation of specific angular momentum (λ_c) as a function of the logarithmic sonic point location (x_c) for a given viscosity parameter

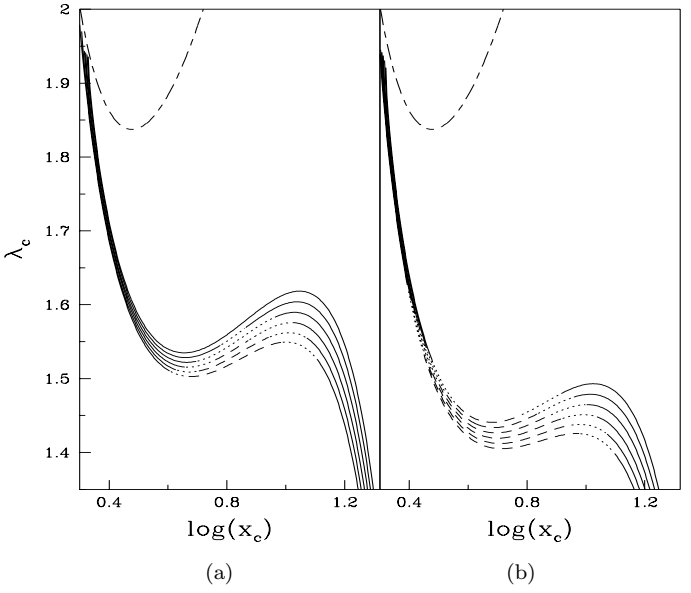

Fig. 1. Variation of specific angular momentum (λ_c) as a function of the logarithmic sonic point location (x_c) for the viscosity parameter (a) $\alpha_\Pi = 0.1$ (left panel) and (b) $\alpha_\Pi = 0.5$ (right panel). Dimensionless accretion rate $\dot{m} = 1.0$ and energy at the sonic point $\mathcal{E}_c = 0.0013$ are chosen. Long-dashed-dotted curve in the upper part is the Keplerian angular momentum distribution. Solid curves represent the saddle type sonic points, dotted curves represent the nodal type sonic points and the short-dashed curves are for the spiral type sonic points. The Comptonization cooling factor ζ is 1 (bottom curve), 20, 40, 60, 80 and 100 (top curve) respectively. Clearly, higher cooling and higher viscosity remove the outer sonic points. Eventually the disk becomes a Keplerian disk passing through the inner sonic point.

($\alpha_\Pi = 0.1$), and dimensionless accretion rate (made dimensionless by the Eddington rate) $\dot{m} = 1.0$ and a given specific energy $\mathcal{E}_c = 0.013$ at the sonic points. The variable used in cooling efficiency factor ζ (Eq. (6a)). From the bottom curve to the top, $\zeta = 1$, 20, 40, 60, 80 and 100 respectively. In Fig. 1(b), the same curve is shown for $\alpha_\Pi = 0.5$, other parameters remaining the same. The long-dashed curve at the top represents the Keplerian angular momentum distribution which is completely independent of the initial flow parameters and depends only on the geometry. Solid part of the curves represents the saddle type sonic points, dotted curve represents the nodal type sonic points and the short-dashed curves are for the spiral type sonic points. Here, at a higher viscosity, the number of sonic points becomes three even with very low angular momentum. For no Comptonization (lowermost curve), the viscous heating is so strong that only outermost sonic point (solid part of the curve at large radius) exists. Only a large degree of cooling can compensate for the viscous heating to bring back the innermost sonic point.

First, notice that the sonic points occur at angular momentum below Keplerian value. For lower values of cooling at the sonic point, an accretion flow contains all the three types of sonic points in a systematic order: saddle — nodal — spiral — nodal — saddle for monotonic increase of location of sonic points. With the increase of ζ, the region of spiral type sonic points gradually decreases and is finally replaced

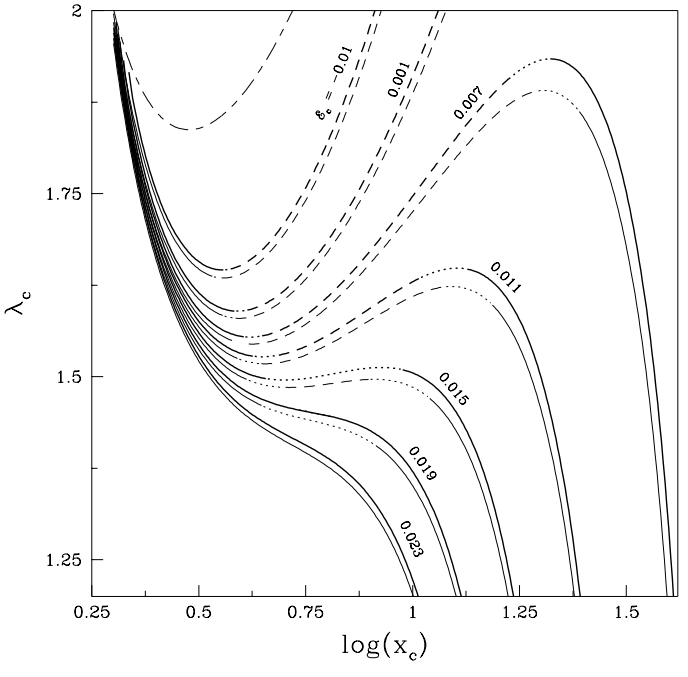

Fig. 2. Variation of the specific angular momentum (λ_c) at the sonic point (x_c) as a function of the specific energy ($\mathcal{E}_c$) of the flow. For each energy, two curves are drawn. The thick curves are drawn for the cases when both the heating and cooling are included while the thin curves are drawn when only the heating is included. For negative energies, there are only two sonic points.

by the nodal type sonic points, though multiple sonic points still exist. For further increase of ζ, all the nodal type sonic points also disappear and are replaced by saddle type sonic points. Note that the angular momentum is always sub-Keplerian. Later, we shall show that when the cooing is very strong, sonic points will form even for super-Keplerian flows.

We continue our investigation of the transonic nature of the flow by showing in Fig. 2 a series of curves where the specific energy at the sonic point is changed (marked). The long dashed curve is the Keplerian distribution as before. Meanings of solid, dashed and dotted curves are the same as before. For negative energies there are two sonic points, the inner one is saddle type (shown in the solid curve) and the dashed curve is the spiral type. For each energy, two curves are drawn. The thick curve is drawn when both the heating and cooling are included while the thin curve is drawn when only the heating is included. The motivation is to impress that the character of a solution can be changed when cooling is included. For instance, the solution for $\mathcal{E}_c = 0.019$ with heating and cooling has no spiral or nodal sonic points. But when the cooling is turned off, the saddle type sonic point becomes nodal type.

In our further study of the nature of the sonic points we draw in Figs. 3(a) and 3(b) the variation of energy at the sonic points with a cooling factor. In Fig. 3(a),

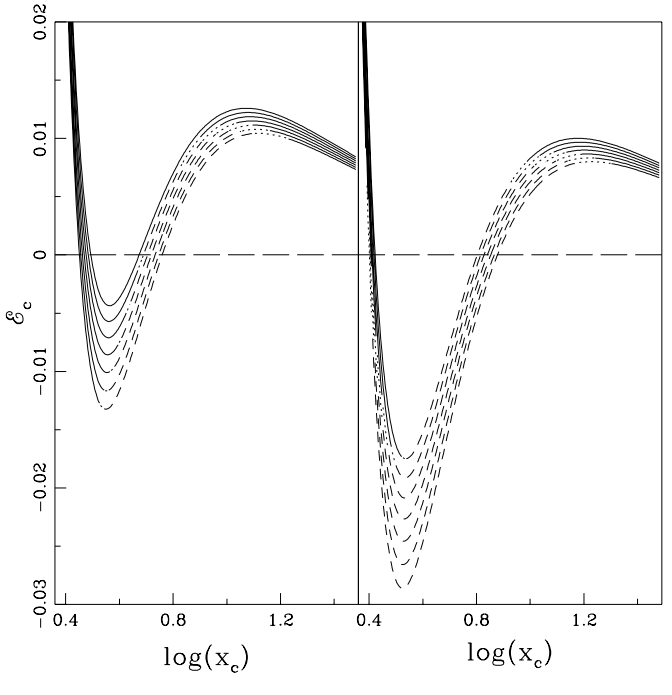

Fig. 3. Variation of the specific energy ($\mathcal{E}_c$) at the sonic point (x_c) as a function of the cooling rate of the flow. (a) $\alpha_\Pi = 0.1$ (left panel) and (b) $\alpha_\Pi = 0.5$ (right panel). For high viscosity, the outer sonic points almost disappear.

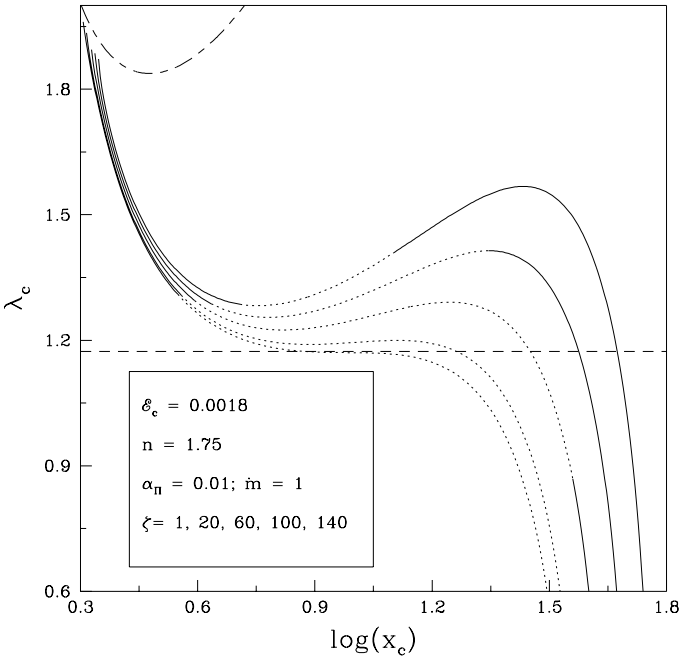

Fig. 4. Recovery of outer sonic point points as cooling process is introduced. Solid and dotted curves are for saddle and nodal type sonic points respectively. Parameters are marked on the plot. Long dashed curve at $\lambda_c = 1.1733$ gives a boundary below which there are no triple sonic points.

low viscosity ($\alpha_\Pi = 0.1$) is used, while in Fig. 3(b), high viscosity ($\alpha_\Pi = 0.5$) is used. Other parameters are: $\lambda = 1.65$ and $\dot{m} = 1$. The curves from bottom to the top are for the cooling factor $\zeta = 1$, 20, 40, 60, 80, 100 and 120. Notice that three sonic points occur only when the specific energy is positive, i.e., for sufficiently hot Keplerian disks or sub-Keplerian flows. For high viscosity, outer sonic points almost disappear from regions close to the black hole.

In Fig. 4, we show how the number of sonic points, reduced due to viscous heating process, is recovered back with the introduction of cooling. The curves are drawn, from the bottom to the top, for $\zeta = 1$, 20, 60, 80 100 and 140 respectively. The solid and dotted curves are for saddle and nodal type sonic points respectively. Other parameters are $\alpha_\Pi = 0.1$ and $\dot{m} = 1$. Polytropic index $n = 1.75$ and specific energy $\mathcal{E} = 0.0018$ are chosen. The long dashed curve gives the boundary of the angular momentum $\lambda_{\rm crit} = 1.1733$ and cooling factor $\zeta = 4.2$, below which there are no triple sonic points, i.e., no shocks in steady flows.

5. Global Solution Topology

Study of shock properties require multi-transonic accretion flow. Accretion flow passes through two different saddle type sonic points and discontinuous jump of the flow variable joins these two different branches — one passes through the inner sonic

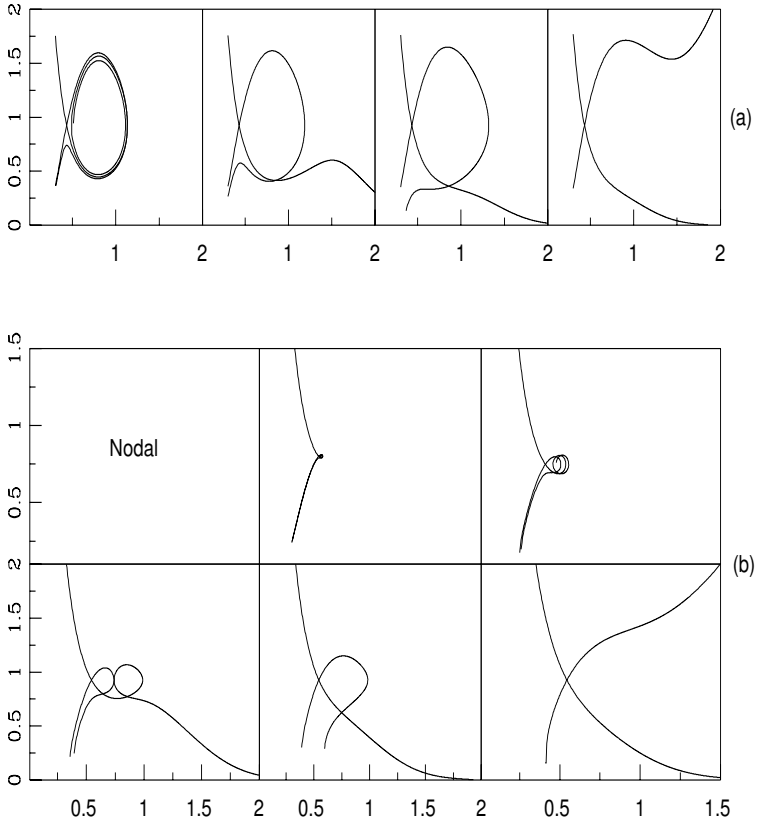

Fig. 5. Solution topologies in presence of heating and cooling. In (a), the parameters are $\zeta = 1$, 10, 25 and 50 respectively. Other parameters are $x_{\rm in} = 2.71$, $\lambda_{\rm in} = 1.68$, $\alpha = 0.01$, $\dot{m} = 0.5$. In (b), the parameters are $\zeta = 1$, 10, 25, 33.1, 50 and 70 respectively. Other parameters are; $x_{\rm in} = 3.5$, $\lambda_{\rm in} = 1.68$, $\alpha = 0.01$, $\dot{m} = 2.0$.

point and the other passes through the outer sonic point. This discontinuous jump usually known as standing shock transition. In this paper, we discuss the nature of solution topology in presence of viscous heating and bremsstrahlung cooling.

In Fig. 5(a), we show how the solution topologies change with cooling. Here we plotted the Mach number as a function of the logarithmic radial distance for $\zeta = 1$, 10, 25 and 50 respectively. Other chosen parameters are: $x_{\rm in} = 2.71$, $\lambda_{\rm in} = 1.68$, $\alpha_\Pi = 0.01$, $\dot{m} = 0.5$ respectively. We note that the topology opens up to allow flows to enter into black holes through the inner sonic points.

In Fig. 5(b), we show six panels in which we assume higher accretion rate and higher inner sonic point locations. The parameters are: $\zeta = 1$, 10, 25, 33.1, 50 and 70 respectively. Other parameters are: $x_{\rm in} = 3.5$, $\lambda_{\rm in} = 1.68$, $\alpha_\Pi = 0.01$, $\dot{m} = 0.2$. Here, as the cooling is increased, the topologies open up similarly, but the route to opening up is different. For instance, the solution in the fourth panel, with $\zeta = 33.1$ is completely new and intriguing. In this case, the flow has the potential to join

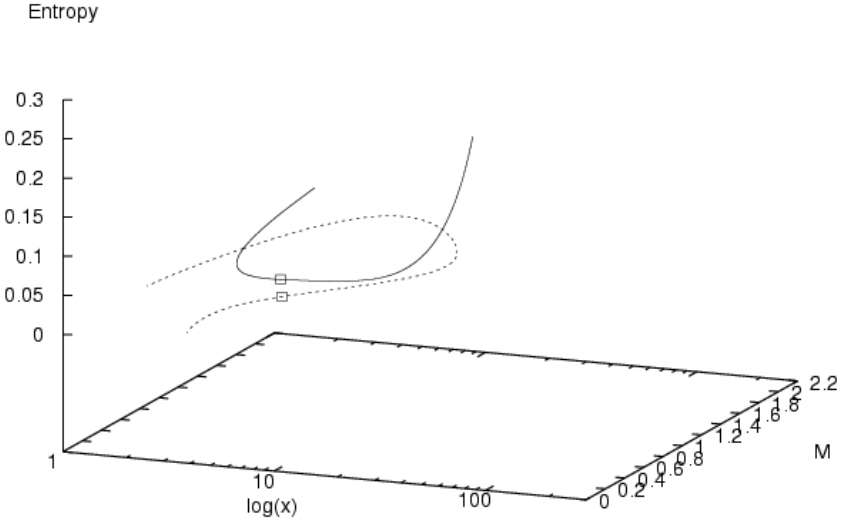

Fig. 6. Three-dimensional plot of the second panel ($\zeta = 10$) of Fig. 5(a) in which the specific entropy is also plotted as it varies along the flow. The boxes represent the pseudo-intersection point of that panel at around $M \sim 0.5$. The two branches have different entropies.

with a Keplerian disk far away (with low Mach number), while at the same time, it also passes through the inner sonic point. But it has multi-valued solution: there are two Mach numbers at a given radial distance in some region. We conjecture that this type of solution should be unstable and would cause non-steady accretion.

Many of these topologies show 'multiple crossings' very similar to what was found in the study of spiral shocks.[3] Actually, since entropy is changing along the flow, the two-dimensional nature of the plots in Fig. 5 is slightly misleading. In Fig. 6, we show a three-dimensional plot of the second panel ($\zeta = 10$) of Fig. 5(a) in which the specific entropy is also plotted as it varies along the flow. In particular, this diagram shows that at the true sonic point, the specific entropy is identical in both the incoming (solid) and outgoing (dotted) branches. But at the 'intersection' (at around $M \sim 0.5$) marked by two squares, the entropies are completely different. Thus, there is no 'sonic point' around $M \sim 0.5$.

6. Parameter Space Description

It is useful to study the global behaviour of the accretion solutions. For this we classify the parameter space spanned by the specific angular momentum and energy at the sonic point. Figure 7 shows the parameter spaces in which the solution passing through the inner sonic point contains a closed spiraling topology as in panel 1 of Fig. 5(a). This means that whether the Rankine–Hugoniot relation is satisfied or not, a shock could form in this region. The shock will be stationary if the Rankine–Hugoniot relation is satisfied[14] and will be oscillating if the relation is not satisfied. The solid, dashed, dot-dashed and dot-long-dashed regions are for

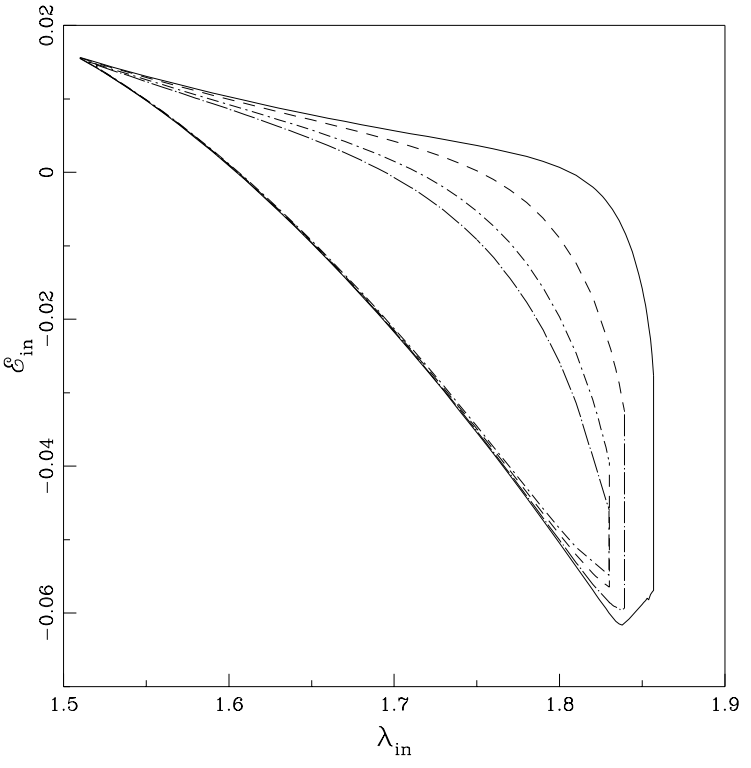

Fig. 7. Region of the parameter space in which the solution passing through the inner sonic point contains a closed spiraling topology. The solid, dashed, dot-dashed and dot-long-dashed regions are for cooling parameter 1, 10, 30, and 50 respectively. Other parameters are $\alpha_\Pi = 0.01$ and $\dot{m} = 0.1$.

cooling parameter 1, 10, 30, and 50, respectively. As the cooling is increased, the region shrinks and becomes smaller and smaller. This indicates that there exists a critical cooling parameter, beyond which a flow will cease to have three sonic points. Other parameters used are $\alpha_\Pi = 0.01$ and $\dot{m} = 0.1$. When the viscosity and cooling are reduced to zero, this region merges exactly to the corresponding region in Ref. 12.

In Figs. 8(a)–(c), we present a few complete solutions which are drawn with the parameters at $\lambda_{\rm in} = 1.7$, $\alpha_\Pi = 0.05$, $\dot{m} = 0.2$ and $\zeta = 5$ and only the inner sonic point is varied: (a) $x_{\rm in} = 2.545$, (b) $x_{\rm in} = 2.55$ and (c) $x_{\rm in} = 2.555$. The corresponding shock locations are (a) $x_s = 48.199$, (b) $x_s = 27.8854$ and (c) $x_s = 18.6445$, respectively. Vertical dashed lines show the shock transitions which connect two solutions, one passing through the inner sonic point and the other passing through the outer sonic point. The spiral loop through the inner sonic point rapidly shrinks with the increase in the sonic point location. The shock location also comes closer. This shows that even though the shock location may change by orders of magnitude, the inner sonic point virtually remains at the same place.

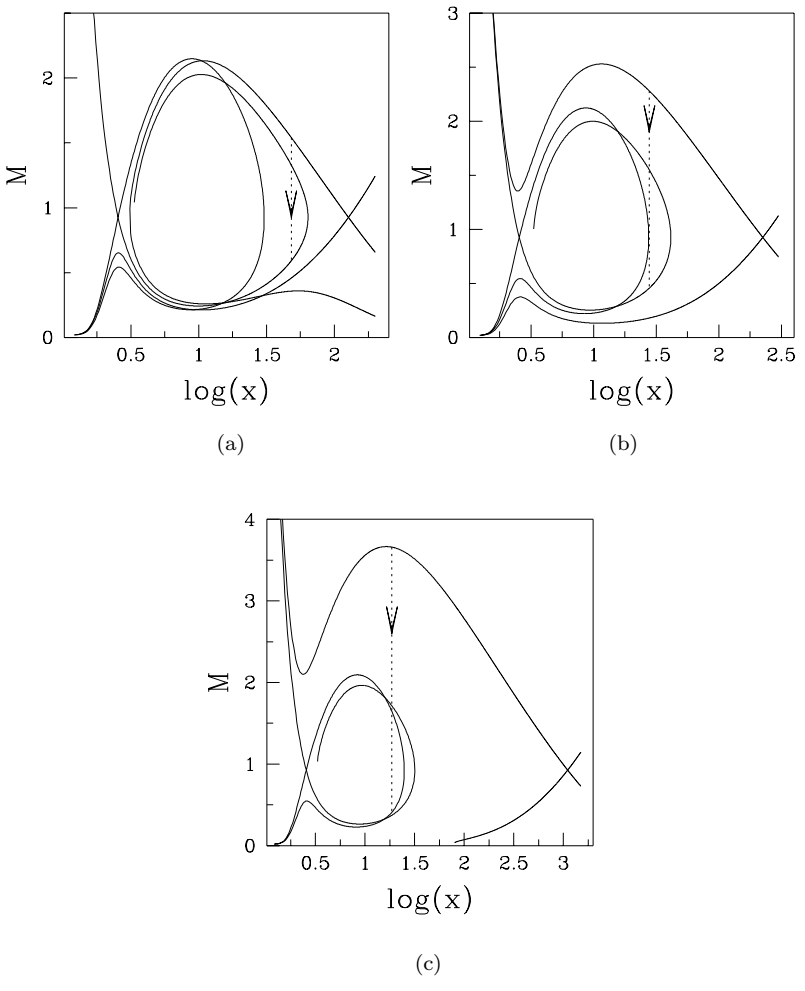

Fig. 8. A few complete solutions which are drawn with the parameters at $\lambda_{\rm in} = 1.7$, $\alpha_\Pi = 0.05$, $\dot{m} = 0.2$ and $\zeta = 5$ and only the inner sonic point is varied: (a) $x_{\rm in} = 2.545$, (b) $x_{\rm in} = 2.55$ and (c) $x_{\rm in} = 2.555$. The corresponding shock locations are (a) $x_s = 48.199$, (b) $x_s = 27.8854$ and (c) $x_s = 18.6445$, respectively. Vertical dashed lines show the shock transitions.

It is instructive to know the sub-division of the parameter space in terms of the topologies of the solutions. All the topologies seen in Paper I are also present in this case, but a new topology occurs (see, Fig. 5(b)) when the cooling is especially strong. Figure 9 shows the sub-division of the parameter space which are marked and the corresponding topologies are shown in the bottom left. When the cooling is very strong, the curve $\mathcal{ABC}$ shows further sub-divisions and a new topology shown in the box C13 occur. The number of loops in the inflow may increase depending on the cooling. The dotted curves indicate that the figure is drawn for different (high) cooling factors ζ. The regions marked S, OS, C11, C12, OAC, I*, O*

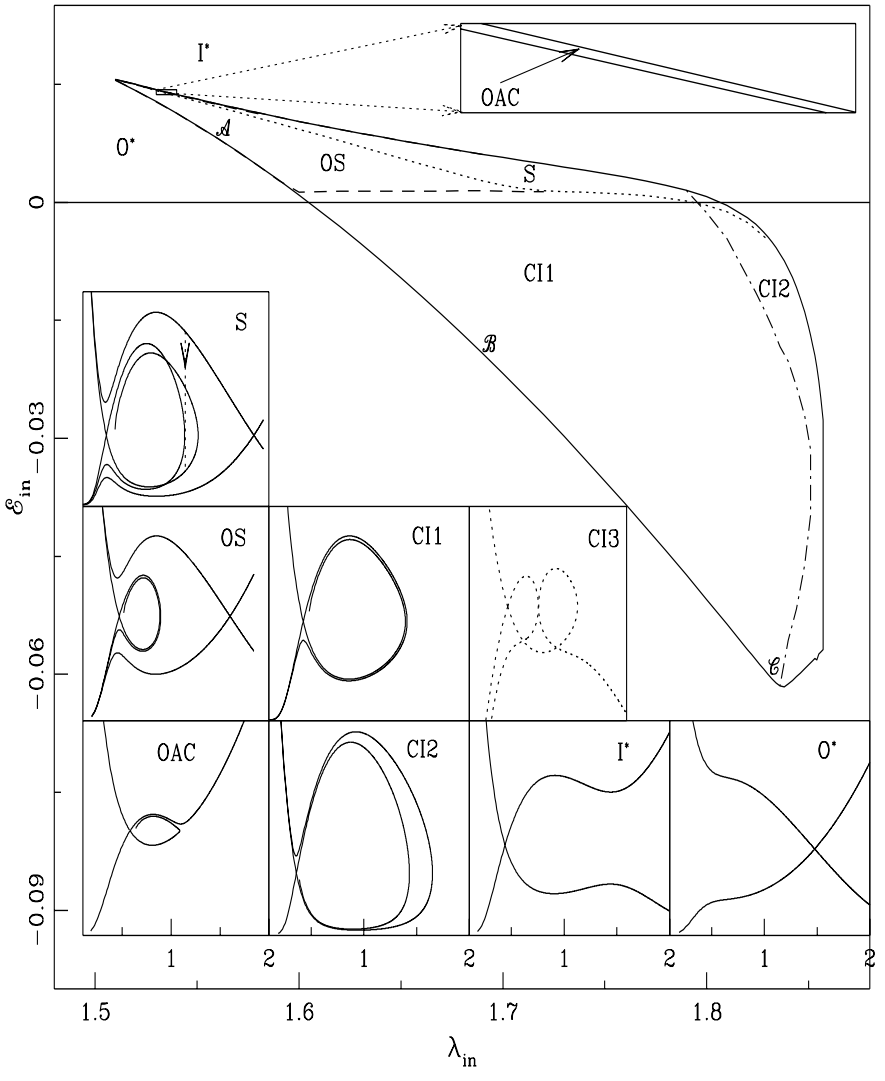

Fig. 9. Division of the parameter space according to the solution topologies shown in the inset. Details are in the text.

produce topologies which produce standing shocks in accretion, oscillating shocks in accretion, region which produces one type of closed topology (clockwise turn), region which produces the other type of closed topology (anti-clockwise turn), region which produces one open and the other closed topology, region which produces open solutions passing only through the outer saddle type sonic point, and the region which produces open solutions passing only through the inner saddle type sonic point respectively. The region producing the new dotted topology C13 is very close to the curve $\mathcal{ABC}$ and can be discernible only when cooling is strong.

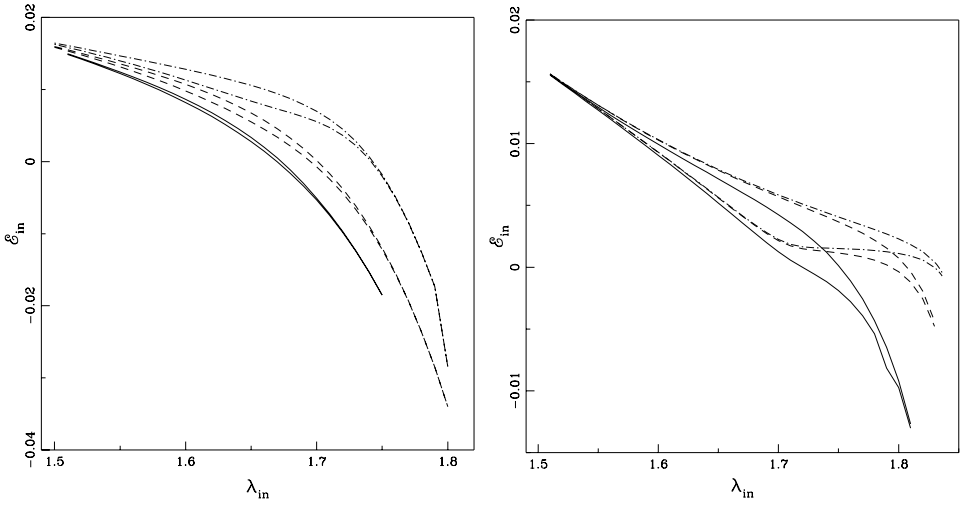

Fig. 10. Modification of the parameter space for shock formation when cooling is varied. (a) $\alpha_\Pi = 0.01$ is chosen and $\zeta = 0.01$, (dot-dashed) 0.1 (long-dashed) and 1 (solid) (left panel). (b) $\alpha_\Pi = 0.05$ is chosen and $\zeta = 1$ (dot-dashed), 5 (long-dashed) and 10 (solid) (right panel).

It would be of interest, to concentrate on the modification of the parameter space for shock formation when cooling is enhanced. In Figs. 10(a) and 10(b) this is shown. In Fig. 10(a), $\alpha_\Pi = 0.01$ is chosen and the cooling parameters are $\zeta = 0.01$, (dot-dashed) 0.1 (long-dashed) and 1 (solid). We note that the region of the parameter space shifts to include negative energy regions as well. (For instance, for $\alpha_\Pi = 0$ and $\zeta = 0$, the parameter space contains only positive energy.) In Fig. 10(b), viscosity parameter is increased to $\alpha_\Pi = 0.05$. This causes a shrinkage in the parameter space. The cooling parameters are $\zeta = 1$ (dot-dashed), 5 (long-dashed) and 10 (solid) respectively. In this case, the parameter space shrinks drastically when cooling is enhanced.

7. Sonic Points for Super-Keplerian Flows?

It is generally accepted that at the sonic points, the flow must be sub-Keplerian.[3] However, if the cooling is very efficient, this requirement may be violated. In Fig. 11, we show that when ζ is very high, of the order of a few hundreds, the sonic point may have angular momentum *above* the Keplerian distribution (dotted curve). Particularly important is that this is possible if the sonic point is located near the black hole horizon. The implication of this is not obvious. Does it mean that very cold flow *can* be Keplerian or super-Keplerian throughout its journey? If so, can it spin up the black hole faster that what is presumed so far? This point is to be addressed in future.

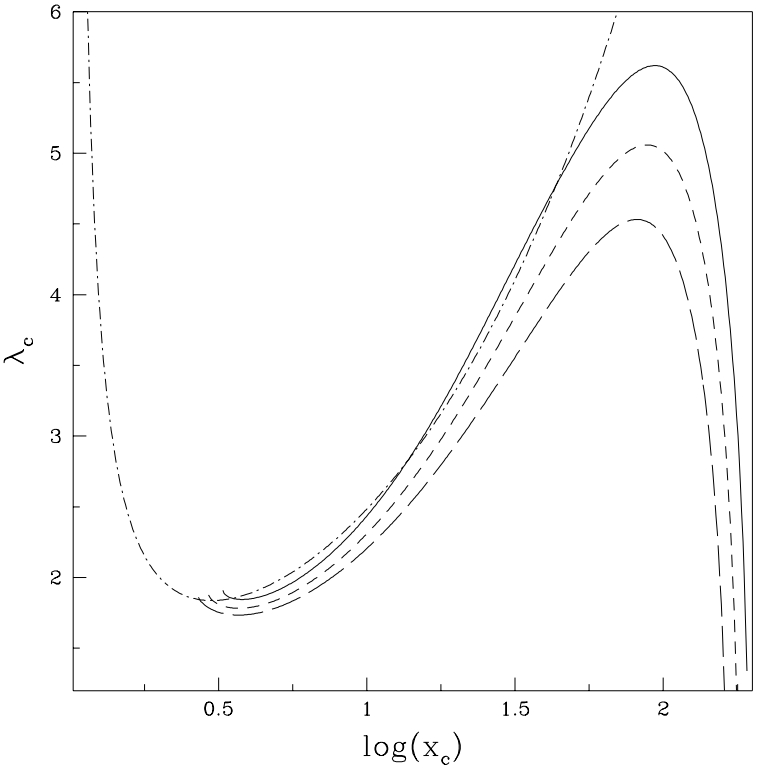

Fig. 11. Example of parameters which produce transonic solutions with super-Keplerian angular momentum. The dot-dashed curve is the Keplerian distribution. Solid curves, from the bottom to the top, are for $\zeta = 400$, 500 and 600 respectively.

8. Critical Cooling and Sub-Division of the Parameter Space

We have already indicated that cooling and heating have opposite effects in deciding the solution topologies, but one does not *exactly* cancel the other effect. When the cooling is enhanced for a given viscosity parameter, the possibility of shock formation is eventually reduced. This is shown in Fig. 12. Here the critical cooling parameter $\zeta = \zeta_{\rm crit}$ is plotted against the specific angular momentum for two different viscosity parameters. Solid curve is for $\alpha_\Pi = 0.01$ and the dashed curve is for $\alpha_\Pi = 0.05$. All possible inner sonic points are considered. The region below the curve contains topologies which are closed and therefore standing or oscillating shocks could be possible while the region above the curve allows solutions with open topologies. We note that for smaller $\lambda_{\rm in}$, the critical cooling factor is smaller. This is expected since the possibility of shock formation is enhanced with larger $\lambda_{\rm in}$ in general. When α_Π is higher $\zeta_{\rm crit}$ is lower. This indicates a general reduction of the parameter space due to higher viscosity[1] which is not totally compensated for by cooling effects.

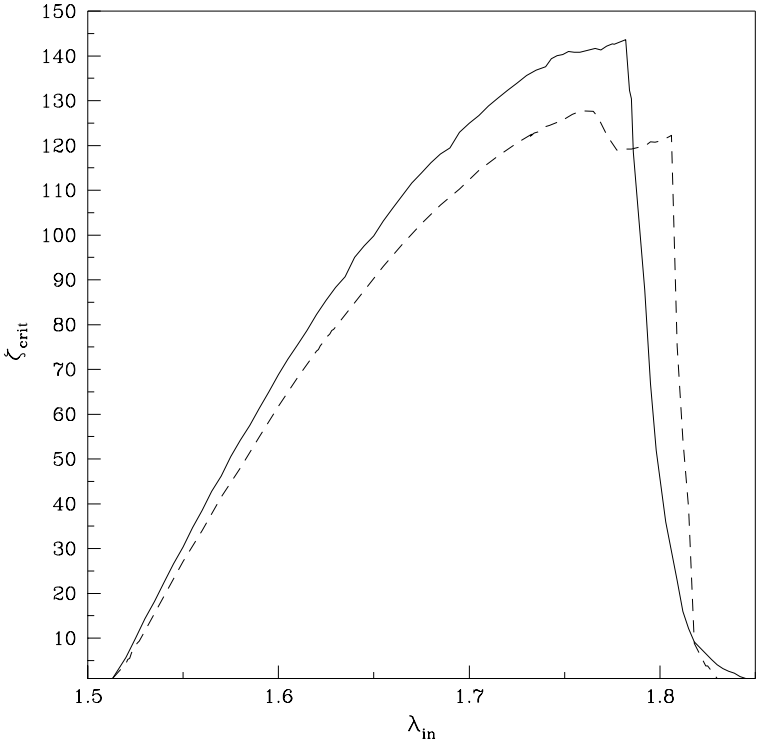

Fig. 12. The variation of the critical cooling parameter as a function of the specific angular momentum at the inner sonic point for two different viscosity parameters. Solid curve is for $\alpha_\Pi = 0.01$ and the dashed curve is for $\alpha_\Pi = 0.05$. The region below the curve contains topologies which are closed and therefore standing or oscillating shocks could be possible while the region above the curve allows solutions with open topologies.

9. Concluding Remarks

In this paper, we studied the dissipative accretion flow in presence of viscous heating and bremsstrahlung cooling processes. Viscosity tends to heat the flow, thereby reducing the Mach number. Cooling, on the other hand, increases the Mach number. Thus, formation of shock, which involves a supersonic to subsonic transition is affected by heating and cooling. We classified the parameter space in terms of whether three sonic points or shocks can form or not. We discovered a completely new topology in which matter, coming from a large distance, is connected to the black hole horizon as a normal solution, but it has multiple valued Mach number solution. We find that cooling can 'undo' the effect of heating on topological properties, only to a certain extent. If the viscosity is high enough, then no matter how much cooling is used, the parameter space shrinks. We have also found that for a given set of flow parameters, there is always a critical cooling factor which separates the parameter space into closed regions, one with a closed and the other with an open topology.

It is generally believed that only the sub-Keplerian flows can pass through the sonic points. However, we find that when the flow is very strongly cooled, even super-Keplerian flows can also pass through the inner sonic point. This is a new result and may be significant in evolution of the spin of the accretion black holes.

Acknowledgment

This work is partly supported by a project (Grant No. SP/S2/K-15/2001) funded by Department of Science and Technology (DST).

References

1. S. K. Chakrabarti and S. Das, *Mon. Not. R. Astron. Soc.* **349**, 649 (2004).
2. S. K. Chakrabarti, *Astrophys. J.* **464**, 664 (1996).
3. S. K. Chakrabarti, *Astrophys. J.* **362**, 406 (1990).
4. S. K. Chakrabarti and L. G. Titarchuk, *Astrophys. J.* **455**, 623 (1995).
5. D. Molteni, H. Sponholz and S. K. Chakrabarti, *Astrophys. J.* **457**, 805 (1996).
6. S. K. Chakrabarti and S. G. Manickam, *Astrophys. J.* **531**, L41 (2000).
7. D. M. Smith, W. A. Heindl, C. B. Markwardt and J. H. Swank, *Astrophys. J.* **554**, L41 (2001).
8. D. M. Smith, W. A. Heindl and J. H. Swank, *Astrophys. J.* **569**, 362 (2002).
9. B. Paczyński and P. J. Wiita, *Astron. & Astrophys.* **88**, 23 (1980).
10. S. K. Chakrabarti, *Theory of Transonic Astrophysical Flows* (World Scientific, Singapore, 1990).
11. R. Matsumoto, S. Kato, J. Fukue and A. T. Okazaki, *Pub. Astron. Soc. Japan* **36**, 7 (1984).
12. S. K. Chakrabarti, *Astrophys. J.* **347**, 365 (1989).
13. S. Das, I. Chattopadhyay and S. K. Chakrabarti, *Astrophys. J.* **557**, 983 (2001).
14. L. D. Landau and E. D. Lifshitz, *Fluid Mechanics* (Pergamon, New York, 1959).